Unraveling the origin of unusual Cs atom disorder in cesium octahedral molybdenum halide cluster compounds, $Cs_2[\{Mo_6X^i_8\}X^a_6]$ (X = Cl and Br)

Norio Saito,[a,b] *Stéphane Cordier,*[c] *Takeo Ohsawa,*[a,d] *Noriko Saito,*[a,d] *Takahiro Takei,*[b] *Fabien Grasset,*[a,e] *Jeffrey Scott Cross,*[f] *Naoki Ohashi*[a,d,e,g,*]

[a] NIMS-CNRS-Saint-Gobain International Collaboration Center, National Institute for Materials Science (NIMS), 1-1 Namiki, Tsukuba, Ibaraki 305-0044, Japan

[b] Center for Crystal Science and Technology, University of Yamanashi, 7–32 Miyamae, Kofu, Yamanashi 400-8511, Japan

[c] Univ Rennes, CNRS, ISCR, Institut des Sciences Chimiques de Rennes–UMR6226, F-35000 Rennes, France

[d] Research Center for Electronic and Optical Materials, NIMS, 1-1 Namiki, Tsukuba, Ibaraki 305-0044, Japan

[e] CNRS-Saint-Gobain-NIMS, IRL3629, Laboratory for Innovative Key Materials and Structures (LINK), NIMS, 1-1 Namiki, Tsukuba, Ibaraki 305-0044, Japan

[f] School of Materials and Chemical Technology, Department of Materials Science and Engineering, Tokyo Institute of Technology, 2-12-1 Ookayama, Meguro, Tokyo 152-8551, Japan

[g] Materials DX Research Center for Element Strategy, Tokyo Institute of Technology, 4259 Nagatsuta, Midori-ku, Yokohama 226-8503, Japan

Corresponding author's email: OHASHI.Naoki@nims.go.jp

ABSTRACT

In this study, we investigate structural disorder and its implications in metal cluster (MC)-based compounds, specifically focusing on $Cs_2[\{Mo_6X^i_8\}X^a_6]$ (X = Cl and Br). Utilizing synchrotron radiation X-ray diffraction, Fourier transform infrared spectroscopy, and luminescent measurements, we examined the incorporation of water molecules into these compounds and their effects on the crystal structure and optical properties. Our findings reveal that the presence of water molecules induces the lattice disorder, particularly the displacement of Cs atoms. Density functional theory calculations, including dispersion corrections (DFT-D), were employed to model superlattices incorporating varying positions and amounts of water molecules. The DFT-D results corroborated experimental data, indicating that water molecules notably impact the lattice structure by causing the Cs disorder without altering the fundamental trigonal arrangement of MC units. Our results reveal that the composition of the compounds, specifically the $Cs/[\{Mo_6X^i_8\}X^a_6]$ ratio, remains stoichiometry, regardless of the amount of water in their lattice. Luminescent spectroscopies confirmed that the water incorporation and the lattice disorder had little effect on the luminescence wavelength, but purification enhanced the luminescent efficiency. This study highlights the importance of understanding structural disorders in MC-based compounds for optoelectronic applications and demonstrates the utility of DFT calculations in exploring complex crystallographic phenomena.

Keywords: Molybdenum cluster; Crystal structure; DFT; Hygroscopic; Disorder.

1. Introduction

Metal atom clusters are defined as finite groups of three to a dozen or more metal atoms held together by direct bonds, typically coordinated by non-metal atoms to form metal cluster-based complexes (MCs).[1,2] These clusters form various polyhedral structures and exhibit a range of interesting properties due to their unique arrangements. Specifically, octahedral molybdenum halide clusters, with the general formula $[\{Mo_6X^i_8\}X^a_6]^{2-}$ (X = Cl, Br, and I), represent a class of classical MCs used as molecular building blocks in constructing inorganic compounds,[3–5] nanomaterials,[6–8] and supramolecular architectures.[9,10] In those MCs, the Mo_6 cluster is coordinated by eight face-capping inner halogen ligands (X^is) and six apical halogen ligands (X^as). According to investigations on the electronic structures of the MCs,[11,12] the roles of X^is and X^as are distinctly different due to their chemical nature: the less negatively charged X^is stabilize the rigid $\{Mo_6X^i_8\}^{4+}$ cluster core, whereas the more ionic X^as interact with external entities, such as solvent molecules and counter cations. Indeed, photoemission spectroscopy enables us to distinguish halogens occupying X^a and X^i sites via differences in electron binding energies.[13,14] Because of the relatively weaker bonding of $Mo{-}X^a$, solution processes for the substitution of X^a by other halogens,[15,16] inorganic anions,[17–20] and organic ligands[21,22] have been proposed, leading to diverse molecular structures for the MCs. Additionally, the unique electronic structure and properties of the MCs and solid-state MC-based compounds highlight their significant potential for applications in optoelectronics, such as red-luminescence phosphors with a large Stokes shift,[23–25] photocatalysts for water reduction,[26] and photosensitizers in photovoltaic solar cells.[27,28]

The electronic structure stability of the $[\{Mo_6X^i_8\}X^a_6]^{2-}$ complexes is a notable characteristic. For instance, photoluminescence spectra for trigonal $Cs_2[Mo_6Cl_{14}]$ and monoclinic $Cs_2[Mo_6Cl_{14}]\cdot H_2O$ are almost identical despite differences in composition and structure.[29,30] This

indicates that the Mo_6 cluster is well-screened by 14 halogens, and its electronic structure is highly isolated from surrounding environments, such as the choice of counter cations and crystallization molecules. Hence, we can consider the $[\{Mo_6X^i_8\}X^a_6]^{2-}$ cluster anionic unit as robust building blocks for designing complex structures. In addition, the relatively large dimension of the $[\{Mo_6X^i_8\}X^a_6]^{2-}$ leads to variations in crystal structures involving these complexes. Various solvate crystals involving the $[\{Mo_6X^i_8\}X^a_6]^{2-}$ complex have been reported: for instance, MC compounds trapping some organic crystallization molecules, such as $Cs_2[Mo_6Cl_{14}]\cdot 6C_3H_6O$ and $Cs_2[Mo_6Cl_{14}]\cdot 4CH_2Cl_2$, can be synthesized.[31] The formation of such solvate compounds is enabled by the relatively large dimension of the $[\{Mo_6X^i_8\}X^a_6]^{2-}$ complex, which makes large interstitial spaces. It should also be noted that $[\{Mo_6X^i_8\}X^a_6]^{2-}$ complexes behave as hard spheres with rigid ionic charge, forming highly ionic chemical bonds with counter cations. Because of these characteristics, investigations on MC-based compounds mostly focus on exploring new crystal structures or new functionality.

Although exploratory studies on compounds involving the $[\{Mo_6X^i_8\}X^a_6]^{2-}$ complex have been extensively performed, attention has not been paid to their purity and structural disorders. As the solid-state compounds involving the $[\{Mo_6X^i_8\}X^a_6]^{2-}$ complex are characterized by their bright luminescence, numerous studies on the utilization of these compounds as phosphors have been reported.[2,6,21,24,25,32–34] However, the effect of purity, such as luminescence quenching induced by structural disorder, has not been discussed in detail, although luminescence quenching is an important issue in conventional inorganic phosphor compounds. For instance, $CsCu_2I_3$ is attracting interest because of its bright luminescence originating from the annihilation of trapped excitons,[35–37] but $FACu_2I_3$, where formamidinium (FA) is substituted for Cs in $CsCu_2I_3$, exhibits no luminescence.[38] This luminescence quenching has been attributed to electronic interaction

between the one-dimensional $[Cu_2I_3]^-$ chain and FA. Although the Mo_6 cluster in the MCs is well screened, as mentioned above, it is presumable that interaction between the MCs and counter cation could cause energy dissipation. Indeed, we have observed elongation of luminescence lifetime in $Cs_2[Mo_6Cl_{14}]$ after dehydration treatment.[30] Hence, we suppose consideration of lattice defects and impurities on the luminescence of the MC compounds is necessary for their future development, particularly for optical applications.

Here, it is interesting to introduce the structural disorder in $Cs_2[\{Mo_6Br^i_8\}Br^a_6]$[39] and reentrant transition in $((n\text{-}C_4H_9)_4N)_2[\{Mo_6Br^i_8\}Br^a_6]$.[40] Crystal structure analyses of $Cs_2[\{Mo_6Br^i_8\}Br^a_6]$ suggest that Cs in $Cs_2[\{Mo_6X^i_8\}X^a_6]$ shows site-split and, in particular, $Cs_2[\{Mo_6Br^i_8\}Br^a_6]$ exhibits a disordered structure due to an obviously large occupation factor at an interstitial site, as illustrated in Fig. 1. According to the refined structural parameters of $Cs_2[\{Mo_6Br^i_8\}Br^a_6]$, this compound is non-stoichiometric with Cs in excess, expressed by $Cs_{2.04}[\{Mo_6Br^i_8\}Br^a_6]$. However, the reason and role of the Cs disorder in the physical and chemical properties have not been investigated in detail. If this non-stoichiometry has physical significance, we have to consider the charge compensation mechanism that enables the excess of Cs. In addition, $(n\text{-}C_4H_9)_4N)_2[\{Mo_6Br^i_8\}Br^a_6]$ exhibits reentrant transition at low temperature, and the luminescence lifetime of this compound changes along with its reentrant transition behavior. Hence, there are examples of lattice disorder and modification of luminescence behavior due to changes in counter cation arrangement.

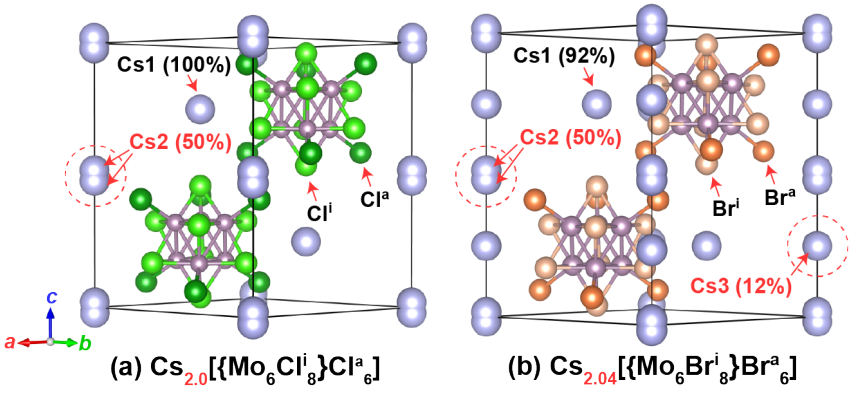

Figure 1. Crystal structures of trigonal phase (a) CMCC and (b) CMBB illustrated based on the crystal structure data reported by refs. 48 and 39, respectively. They exhibit a close-packed hexagonal stacking arrangement with centrosymmetry (space group $P\bar{3}1c$). The red dashed circles denote the disorder of Cs sites. The value in parentheses for each Cs site indicates its atomic occupancy. The unit cell, represented by the black line, contains two MC units ($Z = 2$). The total occupancy (2.04) of the Cs atoms in CMBB significantly exceeds the stoichiometric value of 2.0, while that of CMCC closely aligns with the stoichiometric value.

In this context, we investigate the structural disorder reported for $Cs_2[\{Mo_6X^i_8\}X^a_6]$ (X = Cl and Br). As hydration is the most probable reason for structural disorder in MC-based compounds, we focus on the insertion of water molecules into these MC compounds. Hence, we examined the effect of dehydration treatment on the detailed crystal structure parameters by X-ray diffraction analysis using synchrotron radiation, as well as on the luminescence properties. Furthermore, we conducted density functional theory (DFT) calculations, which simulated superlattices of water molecule-incorporated $Cs_2[\{Mo_6X^i_8\}X^a_6]$ with varying amount and positions of the water molecules. The dispersion correction formalism (DFT-D) was used in DFT calculations to obtain realistic results. These investigations rationalized significant water molecule residues remaining

in $Cs_2[\{Mo_6X^i_8\}X^a_6]$. Notably, DFT-D calculations predict that water molecules in the trigonal lattice structure specifically induce the disorder of the Cs atoms.

2. Materials and method

2.1 Sample preparation

The MC-based compounds, $Cs_2[\{Mo_6X^i_8\}X^a_6]$ (X = Cl and Br), were prepared using methods derived from refs. 39 and 41. The crude solids were dissolved in acetone and crystallized with a rotary evaporator. As this process can induces the incorporation of water molecules into the crystal structure of the MC-based compounds,[29,30] the as-crystallized samples were washed with anhydrous 1-propanol at 25 °C for 24 h to achieve dehydration,[30] and the resulting precipitate was dried under vacuum at 25 °C. The solids were further dried by heating at 300 °C for 1 h under a stream of dry high-purity N_2 gas. In later sections, we abbreviate $Cs_2[\{Mo_6Cl^i_8\}Cl^a_6]$ and $Cs_2[\{Mo_6Br^i_8\}Br^a_6]$ as CMCC and CMBB, respectively.

2.2 Characterization

The crystal structure of the prepared materials was characterized by high-resolution powder X-ray diffraction utilizing synchrotron radiation (SR-XRD) performed at the BL15XU beamline at the Japanese national synchrotron facility, SPring-8. For SR-XRD measurements, monochromatic X-rays at 18.986 keV (λ = 0.653 Å; calibrated with the Nb-*K* absorption edge) were used as the incident beam, and a Debye-Scherrer setup was applied to the sample, which was placed inside a glass capillary with a diameter of 0.2 mm. The lattice parameters of the compounds were calculated using the least squares method with more than ten diffraction signals. The structure refinement

with isotropic atomic displacement parameters (ADPs) was carried out using the Rietveld method.[42,43] All diffraction measurements mentioned above were performed at 300 K.

The presence of water molecule residues in the prepared compounds was characterized by Fourier transform infrared (FT-IR) spectroscopy. The FT-IR measurement was performed using a Nicolet iS50 spectrometer (Thermo Fisher Scientific K.K) with a diffuse reflectance setup. The sample was diluted by mixing it with dried KBr powder in a weight ratio of sample:KBr = 1:20.

Photoluminescence (PL) and time-resolved PL (TR-PL) spectroscopies were conducted using a pulsed laser (100 fs in pulse width and 1 kHz in repetition frequency) generated from an optical parametric amplifier (Spectra Physics TOPAS Prime) excited by a titanium sapphire regenerative amplifier (Spectra Physics Solstice). The wavelength of the laser pulse was set at 410 nm. Photoluminescence spectra were recorded with a VM 505 monochromator (Acton Research Corp.) and detected with an InGaAs photodiode. The TR-PL spectra were measured using a SpectroPro 300i monochromator (Acton Research Corp.) and a C5680 streak camera equipped with a M5677 sweep unit (Hamamatsu Photonics).

2.3 Computational method

Density functional theory calculations were performed to investigate the structural relaxation resulting from the insertion of water molecules into the $Cs_2[\{Mo_6X^i_8\}X^a_6]$ lattice. As shown in Fig. S1, the conventional unit cell of $Cs_2[\{Mo_6X^i_8\}X^a_6]$ is formed by an A-B-A-B close-packed hexagonal stacking and contains two MC units ($Z = 2$). The Cs2 site is at the 2*b* Wyckoff position within layer A. On the other hand, the Cs1 site is at the 2*c* Wyckoff position within layer B, occupying one half of the triangular position. MC units are in another triangular position adjacent to the Cs1 site. According to the previously proposed structural model of CMBB,[39] a partially

occupied Cs site is present within layer B, which is denoted as the Cs3 site. In the present study, we assumed that the water molecules occupy the interstitial sites, either between two Cs2 sites (i.e. the Cs3 site) or between the Cs1 site and the MC unit; the occupancy of Cs atoms at the Cs3 site was assumed to be zero in the computational models in order to maintain stoichiometry and charge neutrality. Since the utilization of small superlattice models may cause an excessively strong interaction between water molecules due to lattice periodicity, we employed superlattice structures containing eight MC units (Z = 8). Although lager superlattice models are better for realism and accuracy, we employed the size of $Z = 8$ due to limitations in computational resources. The initial atomic arrangements in the superlattice model are shown in Fig. S2, where 16 initial structural models before relaxation are exhibited. Superlattice models without water molecule insertion were also adopted to test the simulation conditions and to obtain the electronic and crystal structures of stoichiometric compounds without disorder.

Density functional theory calculations described above were performed using a plane-wave-based pseudopotential method implemented in the CASTEP code,[44] which is included in the Materials Studio software (Dassault Systemes, Tokyo, Japan). The norm-conserving pseudopotentials generated by the CASTEP code and a generalized gradient approximation (GGA) optimized for solids, referred to as GGA-PBEsol,[45] were used as the exchange-correlation functional for the self-consistent calculation of electronic energy minimization. To account for van der Waals (vdW) forces in the total energy calculations, we employed the Tkatchenko-Scheffler formalism[46] for dispersion correction. The plane-wave cut-off energy was set to 1350 eV to ensure simulation accuracy. The convergence tolerance was set to 5.0×10^{-5} nm for atomic displacement, 5.0×10^{-6} eV/atom for total energy, 0.1 eV/nm for maximum interatomic force, and 0.02 GPa for pressure. In the calculation of geometry optimization, the Fletcher–Goldfarb–Shanno Hessian

update scheme[47] was adopted, and no symmetrical restriction was applied to induce complete structural relaxation. The superlattice models with various positions, orientations, and amounts of water molecules were explored to find realistic and stable atomic arrangements in terms of enthalpy.

3. Results and discussion

3.1 FT-IR measurements

The Fourier transform infrared spectra of the obtained samples exhibited a very broad signal corresponding to the O−H stretching mode in the range of 3086−3700 cm^{-1}, as seen in Fig. 2. At the same time, a small peak assignable to the O−H bending mode at 1612−1618 cm^{-1} was found in these spectra. These results clearly indicate the presence of O−H groups (i.e. water and/or alcohol molecules). Figure 2 also shows three strong peaks around 2900 cm^{-1}, which are assignable to the vibrational signals of alkanes (i.e. the C−H stretching mode), likely attributable to 1-propanol molecules still adsorbed on the surfaces of the MC-based compounds.[30] Because of the overlap of the IR signals from the O−H groups of water and 1-propanol molecules, the FT-IR studies could not provide definitive information regarding water molecules incorporated in the MC-based compounds. However, the subsequent SR-XRD measurements reveal the presence of water molecules in the MC-based compounds and suggest that the incorporation of water molecules results in alterations to their crystal structures.

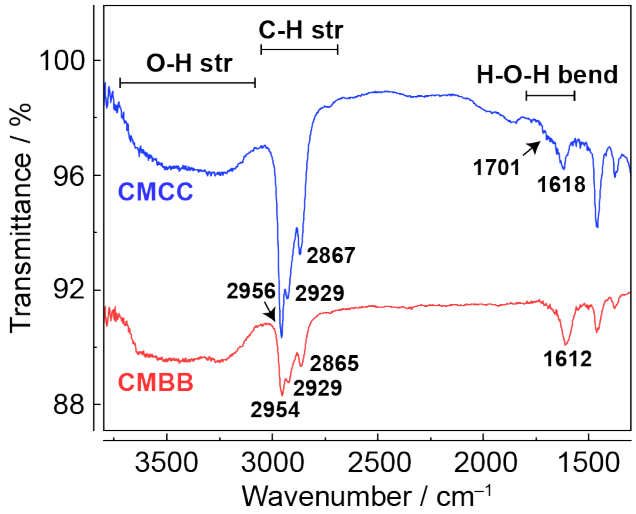

Figure 2. FT-IR spectra of the purified CMCC and CMBB.

3.2 SR-XRD measurements

First, a comparison between the SR-XRD patterns of the hydrated and purified CMCC is shown in Fig. 3. The major phase of the hydrated CMCC sample (see Fig. 3a) was the trigonal phase, but it also contained a monohydrate monoclinic phase[48] as the minor secondary phase. In contrast, the purified CMCC exhibited a single phase of the trigonal phase, as shown in Fig. 3b. The purified CMBB was also a single phase without any trace of a secondary phase (see Fig. 3c). These results indicate that the purification process prevented the formation of hydrated phases. FT-IR spectra of these samples indicate the presence of O−H groups or water molecules even in the purified samples, which were confirmed by SR-XRD to be in the pure trigonal phase without any evident hydrated impurity phases. This suggests that the O−H-related components are inserted in the trigonal phase. Indeed, the refined lattice parameters of the hydrated and purified CMCC, summarized in Table 1, show that the hydrated CMCC exhibited a 0.4% larger unit cell volume than that of the purified CMCC. This result indicates that residual water or O−H groups in CMCC led to an expansion of the trigonal lattice.

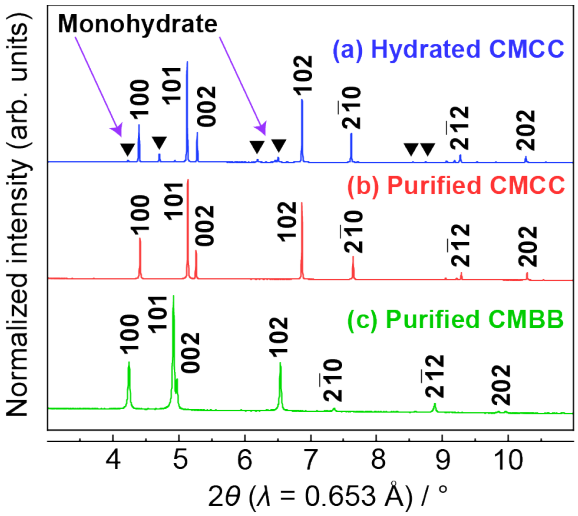

Figure 3. SR-XRD patterns of the (a) hydrated CMCC, (b) purified CMCC, and (c) purified CMBB. The diffraction peaks corresponding to the monohydrated CMCC are marked by inverted triangles.

Table 1. Refined lattice parameters of the hydrated and purified MC-based compounds.

Compound	*a* / Å	*c* / Å	Volume / Å^3
Hydrated CMCC	9.8296(6)	14.1745(7)	1186.07(13)
Purified CMCC	9.7912(3)	14.2238(5)	1180.92(5)
Purified CMBB	10.1754(8)	15.0448(13)	1349.02(18)

To elucidate the possible incorporation of water molecules in the trigonal structure, four structure models illustrated in Fig. S3 were adopted for structural refinements. These models were constructed by considering whether the Cs2 site splits or not and whether the Cs3 site is occupied by an O atom. Here, the O atom located at the Cs3 site represents a water molecule, and the H atoms of the water molecule were omitted due to their very small contribution to diffraction intensity. The results of the structural refinements are shown in Table 2. The value of R_{wp} took the

minimum value when both a split Cs2 site and the presence of O at the Cs3 site were assumed. Hence, it is presumable that the model illustrated in Fig. S3d is the most reasonable assumption. Summary of the results for the structure refinements (Fig. S4 and Table S1) and resulting structure factors (Table S2) deduced by adopting the model shown in Fig. S3d are presented in SI. The most significant improvement in R_{wp} was seen for the hydrated CMCC sample, where R_{wp} was reduced by almost 1% by employing the model for the presence of water at the Cs3 site. This improvement was likely due to the high occupancy of water at the Cs3 site. Indeed, the total occupancy of the O atom at the Cs3 site reached about 90% (Table 2), which is equivalent to the incorporation of approximately one water molecule per MC unit in the hydrated CMCC. In contrast, R_{wp} for the purified CMCC converged well to less than 3.3% and did not change significantly between the four structure models (Table 2). This was likely due to the lower occupancy of water molecules at the Cs3 site, i.e. about 30% in the purified CMCC (see Table 2). This result indicates that even after the dehydration treatment, some water molecules remained at the Cs3 site. Regarding the CMBB sample, R_{wp} was not sensitive to the structural model assumed for refinement. This insensitivity was simply due to the difference in the electron number between Cl and Br. However, the refinement of CMBB implies an occupancy of up to 80% for water molecules at the Cs3 site, even in the purified sample, exhibiting behavior distinct from that of CMCC. This mechanism is clarified through subsequent theoretical calculations.

Table 2. Rietveld refinements of the hydrated and purified MC-based compounds using four structure models illustrated in Fig. S3.

Model	Cs2 split	Occup. of O atom at Cs3	U_{iso} of O atom / Å^2	R_{wp} / %
Hydrated CMCC				
I	No	0	−	7.85
II	Yes	0	−	6.83
III	No	0.95	0.005(4)	6.87
IV	Yes	0.89	0.033(5)	5.88
Purified CMCC				
I	No	0	−	3.28
II	Yes	0	−	3.09
III	No	0.34	0.799(82)	3.22
IV	Yes	0.34	1.020(97)	3.04
Purified CMBB				
I	No	0	−	1.70
II	Yes	0	−	1.68
III	No	0.74	0.084(24)	1.62
IV	Yes	0.81	0.412(44)	1.59

Here, it is interesting to note that the Cs/[{$Mo_6X^i_8$}X^a_6] ratio calculated from the refined occupancy of Cs atoms was identical to the stoichiometry, i.e. 2.0, when the model assuming water insertion was adopted. This is an important observation in terms of charge compensation in the MC-based compounds. In the previously proposed structural models where the Cs3 site was assumed to be occupied by Cs,[39] the chemical composition of the compound clearly exhibits non-

stoichiometry (i.e. Cs/[{$Mo_6X^i_8$}X^a_6] = 2.04). If the excess Cs has physical significance, we need to consider variations in the effective electric charge of the MC units to maintain charge neutrality. However, optical band gaps reported for the MC-based compounds[49,50] have been very reproducible, and there is no solid evidence to prove significant non-stoichiometry in these compounds. We also note that many exploratory studies have reported strong photoluminescence of Cs_2[{$Mo_6X^i_8$}X^a_6].[6,51] As non-stoichiometry in inorganic phosphors typically results in severe luminescence quenching due to excitation energy transfer to quenching sites such as vacancies or impurities,[52,53] the strong luminescence observed in Cs_2[{$Mo_6X^i_8$}X^a_6] prepared under ambient conditions also supports the absence of non-stoichiometry in these compounds. Hence, the present results of the structural refinements, which consider the stoichiometry of Cs/[{$Mo_6X^i_8$}X^a_6], are very reasonable in terms of charge compensation. In addition, we do not need to consider charge compensation mechanisms if impurities are electrically neutral.

3.3 Theoretical calculation

The structure relaxation of the superlattices shown in Fig. S2 was performed using DFT-D calculations, which consider the effects of intermolecular interactions. The fully relaxed superlattice without water molecules, referred to as SL-O, exhibited a lattice volume per MC unit (i.e. V/Z) of 539.6 Å^3 for CMCC and 628.1 Å^3 for CMBB (see Table S3). These volumes are 12.0% for CMCC and 9.0% for CMBB smaller than the corresponding lattice volumes calculated without dispersion correction.[50] This result indicates significant lattice contraction due to the effects of vdW interactions within the MC-based compounds. Table S3 also shows the results of the structure relaxation for superlattices incorporating one to five water molecules. The data indicate that their lattice volumes remained within about ±1% compared to that of SL-O for both CMCC and CMBB,

regardless of the positions and amounts of water molecules. Notably, the packing motif of the MC units in the trigonal lattice remained unchanged during the structure relaxation of the superlattices. These results suggest that the water molecules can be incorporated into the crystal structure of $Cs_2[\{Mo_6X^i_8\}X^a_6]$ without changing its trigonal arrangement. The enthalpy difference (ΔH) between the superlattices with and without water molecules includes contributions from both the water molecules and their different lattice volumes. Therefore, we calculated $\Delta H/nV$, which normalizes ΔH by the lattice volume (V) of the water-incorporated superlattice and the number (n) of water molecules. Table S3 indicates that the normalized enthalpy differences varied within ± a few meV among the superlattices, suggesting that the positions and amounts of water molecules in these superlattices did not significantly impact the relative enthalpy difference. Given the large dimensions of the MC unit, vdW interactions are expected to play a significant role in realistic crystal structures of MC-based compounds. In this context, SL-H is considered the most realistic structure, as it exhibited the smallest lattice volume among all superlattices, despite incorporating four water molecules. Therefore, we focus on SL-H for further analysis.

An analysis of the interatomic distances and angles of water molecules in SL-H clearly indicates that hydrogen bonding interactions between the water molecules and MC units play a crucial role in determining the stable position and orientation of the water molecules. Figure 4 illustrates each interatomic H−X^a distance and angle formed by the O, H, and X^a atoms (∠O−H−X^a) in SL-H for CMCC and CMBB. The H−X^a distances ranged from 2.39 to 2.53 Å for CMCC and 2.56 to 2.73 Å for CMBB. These are significantly shorter than the sum of vdW radii of H and Cl (2.95 Å), and H and Br (3.03 Å),[54] indicating that the MC unit and water molecule interact via hydrogen bonding. Furthermore, the ∠O−H−X^a angles ranged from 156.9° to 166.3° for CMCC and 158.5° to 170.1° for CMBB. These values fall almost within the range of 160° to 180°, which indicates that the

O−H−X^a motif exhibits directional characteristics.[55] The H−X^a bond length and the angle of O−H−X^a thus indicate that the hydrogen bonding interaction between the MC unit and the water molecule determines the position and orientation of the water molecules in the crystal structure of the MC-based compounds.

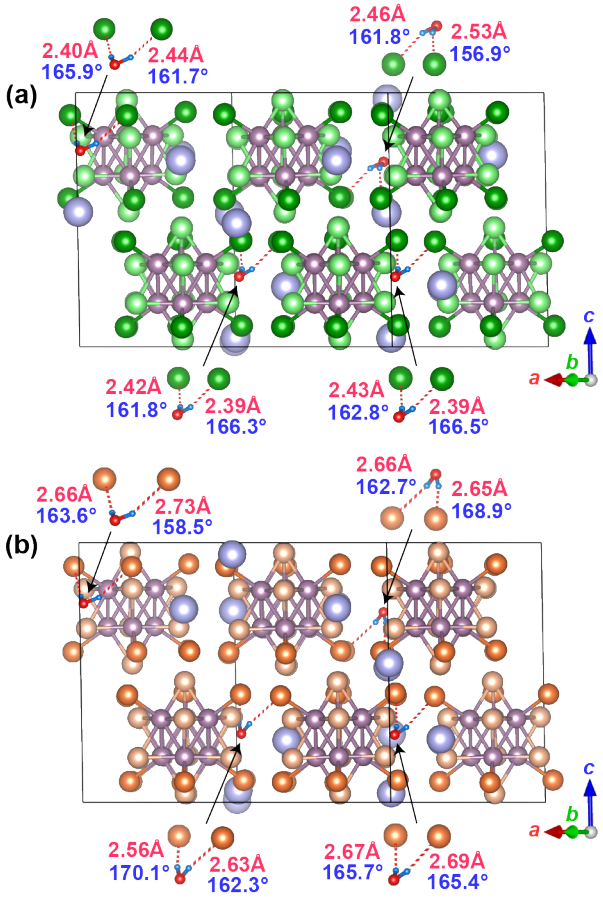

Figure 4. The atomic arrangements in the solid black square shows relaxed crystal structure obtained by DFT-D calculations adopting the SL-H structure shown in Fig. S2. The Atomic arrangements shown outside of the black box show the magnified local structure around the water molecules pointed with black arrows. Interatomic H−X^a distances and angles formed by the O, H, and X^a atoms in SL-H of (a) CMCC and (b) CMBB. The red dot lines indicate the hydrogen bonding of H−X^a. The inset red and blue values show the length of the H−X^a bond and the angle of ∠O−H−X^a, respectively.

For a comparison between the computational and experimentally determined crystal structures, the atomic positions in SL-H were projected into the trigonal unit cell with $Z = 2$. The results of this projection are shown in Fig. 5. Duplicate atoms within a threshold of 0.15 Å were regarded as atoms in the same position during the projection. Indeed, most atoms constituting the MC units were integrated into single individual sites in the trigonal unit cell without any site-splitting. From this result, we reaffirm that the displacements of the MC units due to the incorporation of water molecules remained within the ignorable threshold. In contrast, most Cs atoms were substantially displaced from their original positions beyond the threshold. These Cs atoms were displaced in response to repulsion from the H atoms of adjacent water molecules and attraction to their O atoms. As a result, as shown in Fig. 5, Cs atoms appear to be disordered in the projected unit cell. Characteristics of the Cs atom disorder exhibited significant differences between CMCC and CMBB. In CMCC, Cs1 sites showed relatively minor disorder (disorder A), and Cs2 sites exhibited split-like disorder (disorders B and C), as illustrated in Fig. 5a. In contrast, CMBB additionally revealed a substantial displacement of Cs2 sites, which shifted toward positions near Cs3 sites, resulting in disorders D and E in Fig. 5b. As shown in Fig. S5, displacements of Cs atoms similar to disorders D and E were observed when incorporating more than two water molecules in the CMBB superlattice (i.e. $n/Z \geq 2/8$). This result suggests that the behavior of Cs atom disorder depends on both the halogen composition of the MC unit and the concentration and configuration of water molecules within the crystal structure.

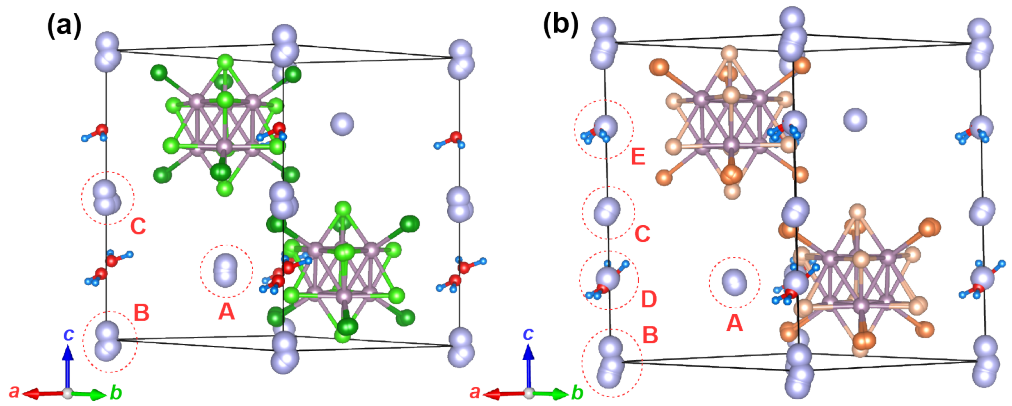

Figure 5. Projections of the water-incorporated superlattices ($Z = 8$) of (a) CMCC and (b) CMBB, which was optimized using DFT-D, into a trigonal unit cell with $Z = 2$. The Cs atom disorders, labeled as A−C for (a) and A−E for (b), are due to the relaxation of the Cs atoms. During the lattice projection, duplicate atoms were removed using a threshold distance of 0.15 Å to obtain a simplified structural representation.

It should be noted that the initial structural model adopted for the DFT-D calculation was constructed by assuming no Cs atoms were present at the Cs3 sites, and only water molecules were placed at Cs3 sites in some superlattice models. However, after relaxation calculations, Cs3 sites were partially occupied by Cs atoms in CMBB, as shown in Fig. S5. Hence, it is evident that Cs in CMBB prefer to occupy the interstitial Cs3 site when water molecule intercalation occurs. Furthermore, the results shown in Fig. S5 demonstrate that occupation of the Cs3 sites by Cs atoms started in one of two models with $n/Z = 2/8$ and in the models with $n/Z = 3/8$. This roughly indicates that occupation of the Cs3 sites starts when the water concentration y in $Cs_2[Mo_6Br_{14}]\cdot yH_2O$ reaches around 0.3.

We tested the plausibility of the DFT-D calculations by optimizing the refinement results of the SR-XRD data using the DFT-predicted structure models. In this test, we assumed that the space

group of the optimized unit cell was *P*31*c*, which allowed us to reproduce the non-uniform disorder illustrated in Fig. 5. We then optimized the number of sites, positions, and occupancy of Cs atoms and compared the results of the optimization to the structure factors of model IV in Table 2. The results of the optimization are summarized in Fig. 6 (and in Table S4 for more detailed results). The optimized unit cell of the hydrated CMCC shown in Fig. 6a seemed to accord with Fig. 5a. Indeed, Cs1 and Cs2 individually split into three distinct sites with a non-uniform occupancy distribution. Notably, the optimized unit cell reduced the R_{wp} value by 0.6% compared to model IV in Table 2. This suggests that the DFT-predicted structure is close to the realistic one. The optimization of the purified CMCC indicated a reduction in the number of Cs2 sites to two, with the occupancy distribution varying to about 50:50. The R_{wp} value was reduced by only 0.2% compared to the refinement using model IV in Table 2. The minor improvement in R_{wp} is rationalized by the low concentration of water molecules in the compound. The purified CMBB also resulted in an R_{wp} value nearly identical to that of model IV in Table 2. However, it still exhibited a significant occupancy (72%) of O near the Cs3 site. Given the consistency with the DFT-predicted structures, this site is likely a mixed state between water molecules and Cs atoms. Therefore, an actual occupancy of water molecules at the Cs3 site in CMBB is likely lower than the refined value.

Considering the results of the plausibility test, we conclude that the characteristic disorder of Cs atoms observed in $Cs_2[\{Mo_6X^i_8\}X^a_6]$ is due to the incorporation of water molecules into the trigonal crystal structure. Remarkably, DFT calculations can accurately predict the water-incorporated crystal structure of $Cs_2[\{Mo_6X^i_8\}X^a_6]$, even including the positions of the disordered Cs atoms.

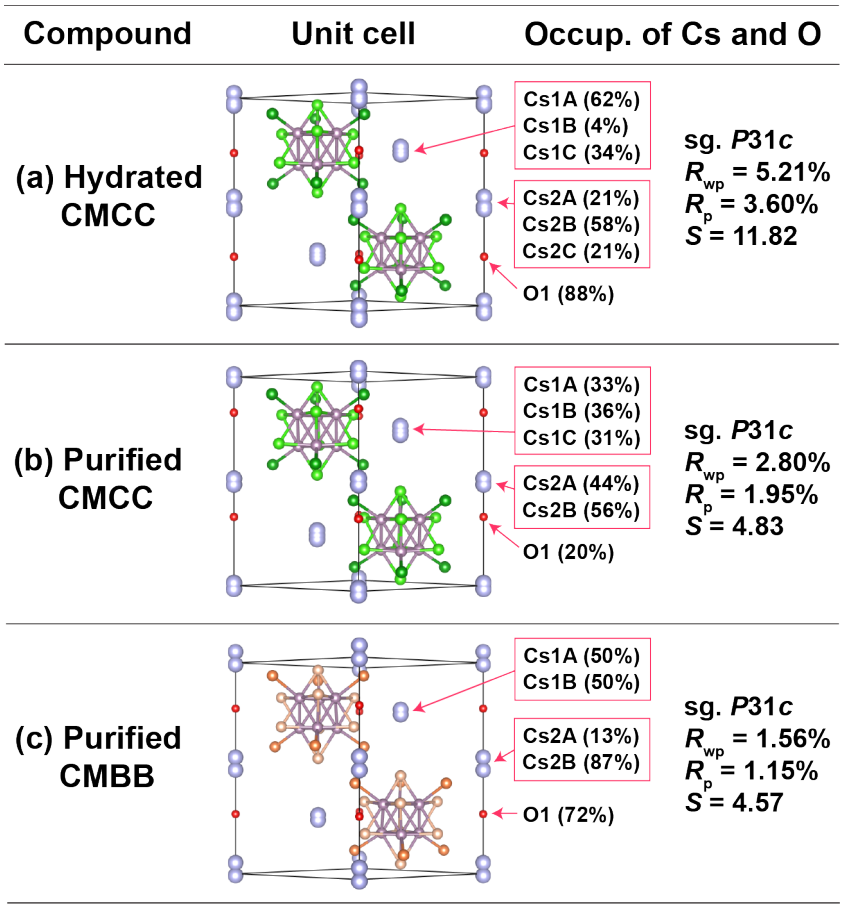

Figure 6. Results of the structure refinements of (a) hydrated CMCC, (b) purified CMCC, and (c) purified CMBB assuming the disorder of the Cs atoms predicted by DFT calculations.

As the random distribution of impurities in solid-state compounds typically alters their luminescence properties,[56,57] we examined the electronic structures in detail. First, we present contour maps of the charge density for water-incorporated CMCC and CMBB superlattices in Figs. 7a and 7b. These maps are prepared for planes involving selected O, H, and X^a atoms. The figures reveal charge distribution between the H and X^a atoms (0.1−0.15 eÅ^{-3}), confirming that the water molecules are bound to X^a via hydrogen bonding.

The projected electronic density of states (PDOS) shown in Figs. 7c and 7d indicates that the total DOS of water-incorporated superlattices appears slightly broadened due to potential

fluctuations caused by the presence of water molecules and disorder in Cs-site occupation. For example, the Cs-5*p* states at −6.81 eV for CMCC split into two peaks due to Cs atom disorder. No defect states appear within the band gaps, as the inserted water molecules are electrically neutral, but a very slight narrowing of band gap due to water insertion, resulting from the broadening of DOS, was confirmed.

It has been reported that the electronic state of the Mo_6 cluster is screened from the external environment, resulting in a luminescence wavelength for trigonal $Cs_2[\{Mo_6Cl^i_8\}Cl^a_6]$ and monoclinic $Cs_2[\{Mo_6Cl^i_8\}Cl^a_6]\cdot H_2O$[30] that is very close despite differences in symmetry and cluster packing density. However, it seems that the PDOS for Mo-*d* around the valence-band maximum (VBM) is affected by water insertion and Cs-site disorder. While the profile of Mo-*d* in the VBM range in pure CMBB (bottom panel in Fig. 7d) is similar to that of pure CMCC (bottom panel in Fig. 7c), those in the superlattice involving water molecule differ from each other. Particularly, the PDOS of Mo-*d* near the VBM in water-inserted CMBB differs from the others. Indeed, the peak maximum of Mo-*d* appears at relatively a shallower range, as indicated by a red arrow in the figure, whereas a deeper peak is higher in the others, as indicated by blue arrows. As the electronic structure of the Mo_6 cluster is essential to the luminescence properties of $[\{Mo_6X^i_8\}X^a_6]^{2-}$, the insertion of water and disorder of Cs sites, resulting in fluctuation of the potential field, may significantly affect the luminescence properties of $Cs_2[\{Mo_6Br^i_8\}Br^a_6]$.

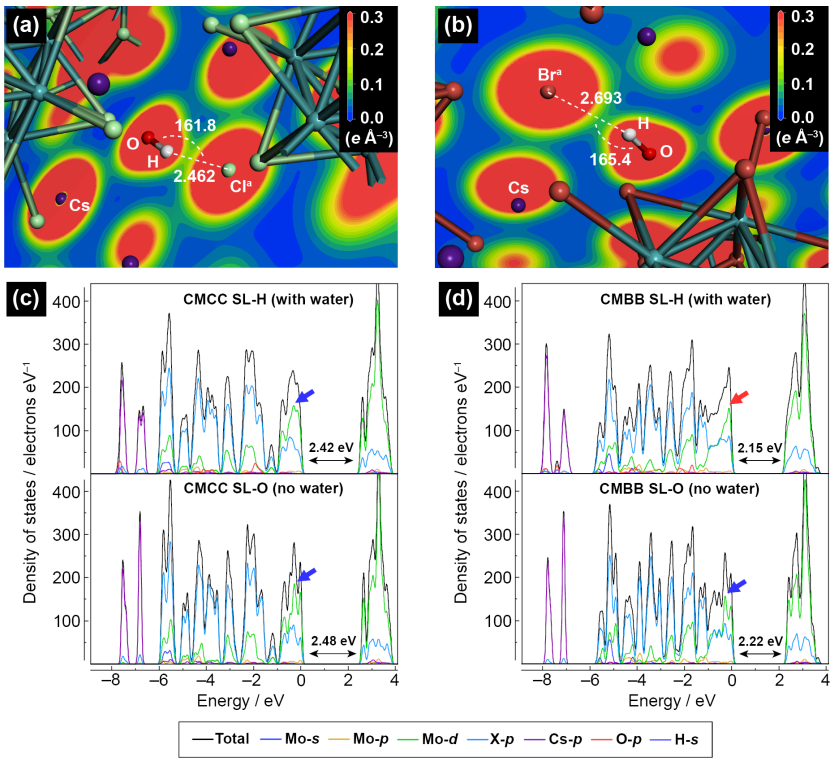

Figure 7. Contour maps of the charge density for water-incorporated (a) CMCC and (b) CMBB, and PDOS of the (c) CMCC and (d) CMBB superlattices with and without water molecules (top and bottom panels, respectively). The blue and red arrows in PDOS indicate the peak maximum of the Mo-*d* state in the VBM range for guides for eyes, by the blue arrow marking the peak maximum located at a relatively deeper level than that indicated by the red arrow.

3.4 Optical and electronic properties

Figure 8a presents the PL spectra of CMCC and CMBB measured at room temperature. Due to the obvious Stokes shift, comparing the calculated energy band gap and luminescence peak is not appropriate. However, the luminescence peak of purified CMCC exhibited a slight blue shift compared to hydrated CMCC, while CMBB showed a red shift compared to CMCC. These results qualitatively align with the calculated energy band gap. Table 3 compares the present results with

the luminescence properties of $[\{Mo_6X^i_8\}X^a_6]^{2-}$ complexes dissolved in acetonitrile.[58] Their emission wavelengths were similar regardless of being in crystalline or solution form, indicating that the Mo_6 cluster was well-screened, resulting in nearly identical emission wavelengths.

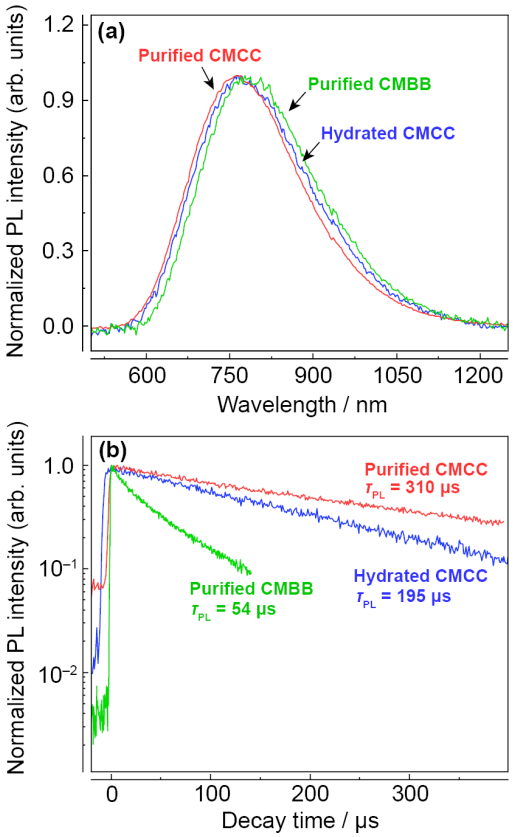

Figure 8. (a) PL and (b) TR-PL spectra of hydrated CMCC, purified CMCC, and purified CMBB. These spectra were measured using the excitation wavelength of 410 nm (Reproduced or adapted with permission from ref. 30. Copyright 2017 RSC Pub).

Table 3. Comparison between the luminescence properties of the present compounds and reference data.

Compounds	PL center / nm	PL lifetime (τ_{PL}) / μs	$1/\tau_{PL} \times 10^3$ / s^{-1}
Hydrated CMCC	769	195±1	5.13
Purified CMCC	764	310±2	3.22
Purified CMBB	782	54±1	18.5
$[\{Mo_6X^i_8\}X^a_6]^{2-}$ complexes dissolved in acetonitrile[58]			
$[Mo_6Cl^i_8Cl^a_6]^{2-}$	764	205	4.88
$[Mo_6Br^i_8Br^a_6]^{2-}$	788	150	6.67

On the other hand, the effect s of water insertion and disorder in Cs distribution are clearly observed in the TR-PL spectra shown in Fig. 8b. These TR-PL spectra were fitted using a single exponential decay function ($I(t) = I_0 \cdot \exp(-t/\tau_{PL})$, where $I(t)$ represents the luminescence intensity at a certain time (t). This resulted in τ_{PL} values of 195±1 μs for hydrated CMCC, 310±2 μs for purified CMCC, and 54±1 μs for purified CMBB. Notably, comparing these τ_{PL} values with references in Table 3 revealed that purified CMCC exhibited a longer τ_{PL} compared to both hydrated CMCC and the $[\{Mo_6Cl^i_8\}Cl^a_6]^{2-}$ acetonitrile solution. Since the inverse of τ_{PL} ($1/\tau_{PL}$) represents the sum of radiative (k_r) and non-radiative (k_{nr}) decay rates and is approximately equal to k_{nr} when $k_{nr} >> k_r$, purified CMCC effectively prevented non-radiative relaxation processes. This indicates that halogens interacting with the surrounding environment contribute to the energy dissipation path, although the luminescence path is localized in the well-screened Mo_6 cluster. It is assumed that the formation of hydrogen bonds through water insertion and the disorder in Cs site occupation led to enhanced non-radiative recombination.

In contrast, purified CMBB exhibited a significantly shorter lifetime compared to the $[\{Mo_6Br^i_8\}Br^a_6]^{2-}$ acetonitrile solution. It should also be noted that the amount of water inserted in hydrated CMCC was estimated to be almost the same as in purified CMBB. The hydrated CMCC exhibited a similar τ_{PL} to the $[\{Mo_6Cl^i_8\}Cl^a_6]^{2-}$ acetonitrile solution, but τ_{PL} of purified CMBB was noticeably shorter than that of the solution. This indicates that the luminescence properties of CMBB are more strongly affected by Cs disorder and water insertion. As described in the previous section, the electronic state (PDOS) of the Mo_6 cluster was evidently affected by disorder. The notably short τ_{PL} of CMBB seems to be consistent with the calculated electronic structure, confirming the relatively high sensitivity of $[\{Mo_6Br^i_8\}Br^a_6]^{2-}$ to the surrounding environment compared to $[\{Mo_6Cl^i_8\}Cl^a_6]^{2-}$.

4. Conclusions

In summary, we investigated the origin of the characteristic Cs atom disorder that observed in $Cs_2[\{Mo_6X^i_8\}X^a_6]$ and its influence on luminescence properties. SR-XRD studies on both purified and hydrated $Cs_2[\{Mo_6X^i_8\}X^a_6]$ (X = Cl and Br) revealed the splitting of the Cs2 site and significant electron residue in the interstitial spaces between Cs2 sites (i.e. the Cs3 site). In terms of charge neutrality, this residue is attributed to water molecules inserted into the crystal structure of $Cs_2[\{Mo_6X^i_8\}X^a_6]$. Even after purification, about 30% occupancy of water was observed in CMCC, while CMBB exhibited a significantly higher occupancy, reaching up to 80%. Results of luminescence measurements indicated that the Mo_6 cluster was well-screened to show almost same luminescence wavelength regardless of the crystalline disorder. As purified CMCC exhibited a significantly longer PL lifetime compared to hydrated CMCC, it was indicated that formation of hydrogen bond between $[\{Mo_6X^i_8\}X^a_6]^{2-}$ and water as well as potential fluctuation resulting from disorder in Cs site are causes for energy dissipation during luminescence process. To understand

the effects of water molecules in the crystal structure, we conducted DFT-D calculations on $Cs_2[\{Mo_6X^i_8\}X^a_6]$ superlattices with varying amount and positions of water molecules. The DFT-D calculations revealed that the incorporation of water molecules did not affect the trigonal lattice motif of the MC units but induced significant displacements of the Cs atoms due to electrostatic interactions with adjacent water molecules. As a result, the water-incorporated superlattices exhibited Cs atom disorders resembling those observed experimentally. The SR-XRD refinements, using the DFT-predicted structure model, effectively reduced the R_{wp} value compared to the conventional model, which suggest that DFT calculations provided more realistic structure. From these results, we conclude that the disorder of the Cs atoms in $Cs_2[\{Mo_6X^i_8\}X^a_6]$ is due to their atomic displacements induced by water molecules without altering the trigonal lattice structure. In addition, this study highlights that DFT calculations can provide essential insights into disorders in MC-based compounds.

Supporting information

Supplemental figures for sample crystal structures; Figures for superlattice models used in DFT calculations; Figures for crystal structure models used in SR-XRD structure refinements; Summary of results of SR-XRD structure refinements; Summary of lattice parameters, enthalpies, and crystal structure figures for DFT calculated superlattices; Structure factors refined using DFT calculated lattice models (PDF).

Crystallographic information files resulted from SR-XRD structure refinements (ZIP).

Acknowledgements

The SR-XRD studies were performed under the approval of the NIMS Beamline Station (Proposal Nos. 2019A4703, 2018A4503 and 2017B4891). Part of this study was performed at the Tokodai

Institute for Elemental Strategy (TIES), supported by the grant number JPMXP0112101001, and performed for the MEXT Program: Data Creation and Utilization Type Material Research and Development Project (No. JPMXP1122683430). The authors also acknowledge valuable discussion with Prof. Jean-François Halet of Rennes Univ., and technical assistance by Dr. Yoshio Katsuya and Masahiko Tanaka of NIMS for SR-XRD measurements.

REFERENCES

[1] Cotton, F. A. Metal atom clusters in oxide systems. *Inorg. Chem.* **1964**, 3, 1217−1220.

[2] Cordier, S.; Grasset, F.; Molard, Y.; Amela-Cortes, M.; Boukherroub, R.; Ravaine, S.; Mortier, M.; Ohashi, N.; Saito, N.; Haneda, H. Inorganic molybdenum octahedral nanosized cluster Units, versatile functional building block for nanoarchitectonics. *J. Inorg. Organomet. Polym*. **2015**, 25, 189−204.

[3] Burdett, J. K.; Lin, J. H. The structures of Chevrel phases. *Inorg. Chem.* **1982**, 21, 5−10.

[4] Perrin, A.; Perrin C. The molybdenum and rhenium octahedral cluster chalcohalides in solid state chemistry: From condensed to discrete cluster units. *CR Chim.* **2012**, 15, 815−836.

[5] Potel, M.; Perrin, C.; Perrin, A.; Sergent, M. New families of ternary molybdenum (II) chlorides with octahedral Mo_6 clusters. *Mater. Res. Bull.* **1986**, 21, 1239−1245.

[6] Grasset, F.; Dorson, F.; Cordier, S.; Molard, Y.; Perrin, C.; Marie, A.-M.; Sasaki, T.; Hajime, H.; Bando, Y.; Mortier, M. Water-in-oil microemulsion preparation and characterization of $Cs_2[Mo_6X_{14}]@SiO_2$ phosphor nanoparticles based on transition metal clusters (X = Cl, Br, and I). *Adv. Mater.* **2008**, 20, 143−148.

[7] Nguyen, N. T. K.; Lebastard, C.; Wilmet, M.; Dumait, N.; Renaud, A.; Cordier, S.; Ohashi, N.; Uchikoshi, T.; Grasset, F. A review on functional nanoarchitectonics nanocomposites based on octahedral metal atom clusters (Nb_6, Mo_6, Ta_6, W_6, Re_6): inorganic 0D and 2D powders and films. *Sci. Technol. Adv. Mater.* **2022**, 23, 547−578.

[8] Nguyen, T. K. N.; Dumait, N.; Grasset, F.; Cordier, S.; Berthebaud, D.; Matsui, Y.; Ohashi, N.; Uchikoshi, T. Zn−Al layered double hydroxide film functionalized by a luminescent octahedral molybdenum cluster: ultraviolet−visible photoconductivity response. *ACS Appl. Mater. Interfaces* **2020**, 12, 40495−40509.

[9] Ivanov, A. A.; Abramov, P. A.; Haouas, M.; Molard, Y.; Cordier, S.; Falaise, C.; Cadot, E.; Shestopalov, M. A. Supramolecular host–guest assemblies of $[M_6Cl_{14}]^{2-}$, M = Mo, W, clusters with γ-cyclodextrin for the development of CLUSPOMs. *Inorganics* **2023**, 11, 77.

[10] Carrasco, I.; Ehni, P.; Ebert, M.; Dumait, N.; Taupier, G.; Amela-Cortes, M.; Roiland, C.; Cordier, S.; Knöller, J. A.; Jacques, E.; Laschat, S.; Molard, Y. Game of crowns: Na^+ is coming! Red NIR-emissive hybrid liquid crystals containing discotic crown ethers and $Na_2Mo_6X_8^iCl_6$ (X^i = Cl or Br). *ACS Appl. Mater. Interfaces* **2023**, 15, 39752–39764.

[11] Li, R.-Z.; Yuan, Q.; Yang, Z.; Aprà, E.; Li, Z.; Azov, V. A.; Kirakci, K.; Warneke, J.; Wang, X.-B. Photoelectron spectroscopy of $[Mo_6X_{14}]^{2-}$ dianions (X = Cl–I). *J. Chem. Phys.* **2019**, 151, 194310.

[12] Müller, P. C.; Schmit, N.; Sann, L.; Steinberg, S.; Dronskowski, R. Fragment orbitals extracted from first-principles plane-wave calculations. *Inorg. Chem.* **2024**, Article ASAP. DOI: 10.1021/acs.inorgchem.4c01024.

[13] Best, S. A.; Walton, R. A. X-ray photoelectron spectra of inorganic molecules. 22. Halogen core electron binding energies of low oxidation state molybdenum bromide and molybdenum iodide clusters and niobium and tantalum chlorides containing the $[M_6Cl_{12}]^{n+}$ cores. *Inorg. Chem.* **1979**, 18, 484–488.

[14] Hamer, A. D.; Walton, R. A. X-ray photoelectron spectra of inorganic molecules. IX. Distinction between bridging and terminal metal-chlorine bonds in metal halide clusters of rhenium(III) and molybdenum(II). *Inorg. Chem.* **1974**, 13, 1446–1451.

[15] Preetz, W.; Harder, K. Synthesis, structure and properties of the cluster anions $[(Mo_6Cl^i_8)X^a_6]^{2-}$ with $X^a \equiv$ F, C1, Br, I. *J. Alloys Compd.* **1992**, 183, 413−429.

[16] Bruckner, P; Preetz, W; Punjer, M. Synthesis, crystal structure, NMR, vibrational spectra, and normal coordinate analysis of the cluster anions $[(Mo_6I_8^i)Y_6^a]^{2-}$, Y^a = F, Cl, Br, I. *Z. Anorg. Allg. Chem.* **1997**, 623, 8−17.

[17] Segura-Sanchis, E.; Moreno, A.; Ramiro-Manzano, F.; Fenollosa, R.; Feliz, M.; Atienzar, P. Optoelectronic properties of octahedral molybdenum cluster-based materials at a single crystal level. *Dalton Trans.* **2023**, 52, 17818−17825.

[18] Segura-Sanchis, E.; Fenollosa, R.; Rodriguez, I.; Molard, Y.; Cordier, S.; Feliz, M.; Pedro, A. Octahedral molybdenum cluster-based single crystals as Fabry–Pérot Microresonators. *Cryst. Growth Des.* **2022**, 22, 60–65.

[19] Marchuk , M. V.; Vorotnikov, Y. A.; Kuratieva, N. V.; Shestopalov, M. A. Cationic cluster complex $[\{Mo_6I_8\}(H_2O)_4(OH)_2]^{2+}$ with diphenyl phosphate anions: Structure and optical properties behavior. *Inorg. Chim. Acta* **2024**, 560, 121819.

[20] Kirakci, K.; Shestopalov, M. A.; Lang, K. Recent developments on luminescent octahedral transition metal cluster complexes towards biological applications. *Coord. Chem. Rev.* **2023**, 481, 215048.

[21] Kirakci, K.; Kubát, P.; Dušek, M.; Fejfarová, K.; Šícha, V.; Mosinger, J.; Lang, K. A highly luminescent hexanuclear molybdenum cluster – A promising candidate toward photoactive materials. *Euro. J. Inorg. Chem.* **2012**, 19, 3107−3111.

[22] Mikhailov, M. A.; Brylev, K. A.; Abramov, P. A.; Sakuda, E.; Akagi, S.; Ito, A.; Kitamura, N.; Sokolov, M. N. Synthetic tuning of redox, spectroscopic, and photophysical properties of $\{Mo_6I_8\}^{4+}$ core cluster complexes by terminal carboxylate ligands. *Inorg. Chem.* **2016**, 55, 8437–8445.

[23] Maverick, A. W.; Najdzionek, J. S.; MacKenzie, D.; Nocera, D. G.; Gray, H. B. Spectroscopic, electrochemical, and photochemical properties of molybdenum(II) and tungsten(II) halide clusters. *J. Am. Chem. Soc.* **1983**, 105, 1878−1882.

[24] Yang, C.; Sheng, W.; Moemeni, M.; Bates, M.; Herrera, C. K.; Borhan, B.; Lunt, R. R. Ultraviolet and near-infrared dual-band selective-harvesting transparent luminescent solar concentrators. *Adv. Energy Mater.* **2021**, 11, 2003581.

[25] Zhao, Y.; Lunt, R. R. Transparent luminescent solar concentrators for large-area solar windows enabled by massive Stokes-shift nanocluster phosphors. *Adv. Energy Mater.* **2013**, 3, 1143−1148.

[26] Feliz, M.; Atienzar, P.; Amela-Cortés, M.; Dumait, N.; Lemoine, P.; Molard, Y.; Cordier, S. Supramolecular anchoring of octahedral molybdenum clusters onto graphene and their synergies in photocatalytic water reduction. *Inorg. Chem.* **2019**, 58, 15443−15454.

[27] Nguyen, T. K. N.; Ishii, S.; Renaud, A.; Grasset, F.; Cordier, S.; Dumait, N.; Fudouzi, H.; Uchikoshi, T. Effect of an aromatic sulfonate ligand on the photovoltaic performance of molybdenum cluster-sensitized solar cells. *ACS Appl. Energy Mater.* **2024**, 7, 760−773.

[28] Renaud, A.; Nguyen, T. K. N.; Grasset, F.; Raissi, M.; Guillon, V.; Delabrouille, F.; Dumait, N.; Jouan, P.-Y.; Cario, L.; Jobic, S.; Pellegrin, Y.; Odobel, F.; Cordier, S.; Uchikoshi, T. Preparation by electrophoretic deposition of molybdenum iodide cluster-based functional nanostructured photoelectrodes for solar cells. *Electrochim. Acta* **2019**, 317, 737−745.

[29] Saito, N.; Wada, Y.; Lemoine, P.; Cordier, S.; Grasset, F.; Ohsawa, T.; Saito, N.; Cross, J. S.; Ohashi, N. Theoretical and experimental determination of the crystal structures of cesium–molybdenum chloride. *Jpn. J. Appl. Phys.* **2016**, 55, 075502.

[30] Saito, N.; Lemoine, P.; Cordier, S.; Wada, Y.; Ohsawa, T.; Saito, N.; Grasset, F.; Cross, J. S.; Ohashi, N. Solvent-mediated purification of hexamolybdenum cluster halide, $Cs_2[Mo_6Cl_{14}]$ for enhanced optical properties, *CrystEngComm* **2017**, 19, 6028−6038.

[31] Saito, N.; Lemoine, P.; Cordier, S.; Matsushita, Y.; Ohsawa, T.; Grasset, F.; Cross, J. S.; Ohashi, N. Structural and electronic properties of the metal cluster-based compounds including high concentration of solvent molecules. *Z. Anorg. Allg. Chem.* **2021**, 647, 1−9.

[32] Molina, E. F.; Jesus, N. A. M.; Paofai, S.; Hammer, P.; Amela-Cortes, M.; Robin, M.; Cordier, S.; Molard, Y. When a Red–NIR-Emissive $Cs_2[Mo_6Br_{14}]$ interacts with an active diureasil–PEO

matrix: design of tunable and white-light-emitting hybrid material. *Chem. A Euro. J.* **2019**, 25, 15248−15251.

[33] Neaime, C.; Amela-Cortes, M.; Grasset, F.; Molard, Y.; Cordier, S.; Dierre, B.; Mortier, M.; Takei, T.; Takahashi, K.; Haneda, H.; Verelstf, M.; Lechevallier, S. Time-gated luminescence bioimaging with new luminescent nanocolloids based on $[Mo_6I_8(C_2F_5COO)_6]^{2-}$ metal atom clusters. *Phys. Chem. Chem. Phys.* **2016**, 18, 30166−30173.

[34] Kuttipillai, P. S.; Yang, C.; Chen, P.; Wang, L.; Bates, M.; Lunt, S. Y.; Lunt, R. R. Enhanced electroluminescence efficiency in metal halide nanocluster based light emitting diodes through apical halide exchange. *ACS Appl. Energy Mater.* **2018**, 1, 3587–3592.

[35] Li, Q.; Chen, Z.; Yang, B.; Tan, L.; Xu, B.; Han, J.; Zhao, Y.; Tang, J.; Quan, Z. Pressure-induced remarkable enhancement of self-trapped exciton emission in one-dimensional $CsCu_2I_3$ with tetrahedral units. *J. Am. Chem. Soc.* **2020**, 142, 1786–1791.

[36] Jun, T.; Handa, T.; Sim, K.; Iimura, S.; Sasase, M.; Kim, J.; Kanemitsu, Y.; Hosono, H. One-step solution synthesis of white-light-emitting films via dimensionality control of the Cs–Cu–I system. *APL Mater.* **2019**, 7, 111113.

[37] Kentsch, R.; Morgenroth, M.; Scholz, M.; Xu, K.; Günne, J. S.; Lenzer, T.; Oum, K. Direct observation of the exciton self-trapping process in $CsCu_2I_3$ thin films. *J. Phys. Chem. Lett.* **2020**, 11, 4286–4291.

[38] Ohashi, N.; Matsushita, Y.; Saito, N. Experimental and theoretical investigation of crystal structure of formamidinium–copper–iodide single crystals grown from aqueous solution. *J. Solid State Chem.* **2022**, 306, 122778.

[39] Kirakci, K.; Cordier, S.; Perrin, C. Synthesis and characterization of $Cs_2Mo_6X_{14}$ (X = Br or I) hexamolybdenum cluster halides: efficient Mo_6 cluster precursors for solution chemistry syntheses. *Z. Anorg. Allg. Chem.* **2005**, 631, 411−416.

[40] Saito, N.; Nishiyama, D.; Matsushita, Y.; Wada, Y.; Cordier, S.; Ohsawa, T.; Grasset, F.; Ohashi, N. Reentrant structural and optical properties of organic–inorganic hybrid metal cluster compound $((n\text{-}C_4H_9)_4N)_2[Mo_6Br^i_8Br^a_6]$. *CrystEngComm* **2022**, 24, 465−470.

[41] Koknat, F. W.; Adaway, T. J.; Erzerum, S. I.; Syed, S. Convenient synthesis of the hexanuclear molybdenum(II) halides Mo_6Cl_{12} and $Mo_6Br_{12}•2H_2O$. *Inorg. Nucl. Chem. Lett.* **1980**, 16, 307−310.

[42] Rietveld, H. M. A profile refinement method for nuclear and magnetic structures. *J. Appl. Crystallogr* **1969**, 2, 65−71.

[43] Kim, Y.-I.; Izumi, F. Structure refinements with a new version of the Rietveld-refinement program RIETAN. *J. Ceram. Soc. Jpn.* **1994**, 102, 401−404.

[44] Clark, S. J.; Segall, M. D.; Pickard, C. J.; Hasnip, P. J.; Probert, M. J.; Refson, K.; Payne, M. C. First principles methods using CASTEP. *Z. Kristallogr* **2005**, 220, 567−570.

[45] Perdew, J. P.; Ruzsinszky, A.; Csonka, L. G. I.; Vydrov, O. A.; Scuseria, G. E.; Constantin, L. A.; Zhou, X.; Burke, K. Restoring the density-gradient expansion for exchange in solids and surfaces. *Phys. Rev. Lett.* **2008**, 100, 136406.

[46] Tkatchenko, A.; Scheffler, M. Accurate molecular van der Waals interactions from ground-state electron density and free-atom reference data. *Phys. Rev. Lett.* **2009**, 102, 073005.

[47] Pfrommer, B. G.; Côté, M.; Louie, S. G.; Cohen, M. L. Relaxation of crystals with the quasi-Newton method. *J. Comput. Phys.* **1997**, 131, 233−240.

[48] Saito, N.; Lemoine, P.; Dumait, N.; Amela-Cortes, M.; Paofai, S.; Roisnel, T.; Nassif, V.; Grasset, F.; Wada, Y.; Ohashi, N.; Cordier, S. From $Cs_2Mo_6Cl_{14}$ to $Cs_2Mo_6Cl_{14}•H_2O$ and vice versa: crystal chemistry investigations. *J. Clust. Sci.* **2017**, 28, 773−798.

[49] Schäfer, H.; Schnering, H.-G. V.; Tillack, J.; Kuhnen, F.; Wöhrle, H.; Baumann H. Neue untersuchungen über die chloride des molybdäns. *Z. Allg. Anorg. Chem.* **1967**, 353, 281−310.

[50] Saito, N.; Cordier, S.; Lemoine, P.; Ohsawa, T.; Wada, Y.; Grasset, F.; Cross, J. S.; Ohashi, N. Lattice and valence electronic structures of crystalline octahedral molybdenum halide clusters-based compounds, $Cs_2[Mo_6X_{14}]$ (X = Cl, Br, I), studied by density functional theory calculations. *Inorg. Chem.* **2017**, 56, 6234–6243.

[51] Costuas, K.; Garreau, A.; Bulou, A.; Fontaine, B.; Cuny, J.; Gautier, R.; Mortier, M.; Molard, Y.; Duvail, J.-L.; Faulques, E.; Cordier, S. Combined theoretical and time-resolved photoluminescence investigations of $[Mo_6Br^i_8Br^a_6]^{2-}$ metal cluster units: evidence of dual emission. *Phys. Chem. Chem. Phys.* **2015**, 17, 28574−28585.

[52] Senden, T.; Dijk-Moes, R. J. A.; Meijerink, A. Quenching of the red Mn^{4+} luminescence in Mn^{4+}-doped fluoride LED phosphors. *Light Sci. Appl.* **2018**, 7, 8.

[53] Yang, P.; Deng, P.; Yin, Z. Concentration quenching in Yb:YAG. *J. Lumin.* **2002**, 97, 51−54.

[54] Alvarez, S. A cartography of the van der Waals territories. *Dalton Trans.* **2013**, 42, 8617−8636.

[55] Kollman, P. A. Theory of hydrogen bond directionality. *J. Am. Chem. Soc.* **1972**, 94, 1837−1842.

[56] Makino, T.; Segawa, Y.; Yoshida, S.; Tsukazaki, A.; Ohtomo, A.; Kawasaki, M. Gallium concentration dependence of room-temperature near-band-edge luminescence in *n*-type ZnO:Ga. *Appl. Phys. Lett.* **2004**, 85, 759–761.

[57] Oh, E.; Park, H.; Park, Y. Influence of potential fluctuation on optical and electrical properties in GaN. *Appl. Phys. Lett.* **1998**, 72, 1848–1850.

[58] Akagi, S.; Fujii, S.; Kitamura, N. A study on the redox, spectroscopic, and photophysical characteristics of a series of octahedral hexamolybdenum(ii) clusters: $[\{Mo_6X_8\}Y_6]^{2-}$ (X, Y = Cl, Br, or I). *Dalton Trans.* **2018**, 47, 1131−1139.

For Table of Contents Only

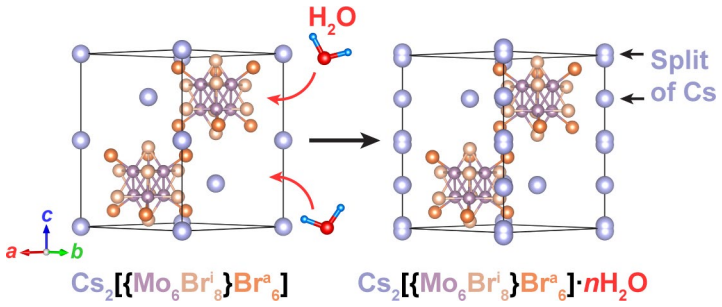

Synopsis

Synchrotron XRD, FT-IR, PL spectroscopies, and DFT calculations reveal that water molecules incorporated into $Cs_2[\{Mo_6X^i_8\}X^a_6]$ induce significant lattice disorder by displacing Cs atoms, thereby reducing the luminescent efficiency, although the fundamental trigonal structure remains intact. Unlike previous studies suggesting non-stoichiometry due to Cs disorder, this study finds that the Cs/$[\{Mo_6X^i_8\}X^a_6]$ ratio remains consistent, even with varying water content in the lattice.